scientific reports

OPEN

The cellular prion protein does not affect tau seeding and spreading of sarkosyl-insoluble fractions from Alzheimer's disease

Julia Sala-Jarque[1,2,3,4,10,11], Vanessa Gil[1,2,3,4,11], Pol Andrés-Benito[3,5], Inés Martínez-Soria[1,2,3,4], Pol Picón-Pagès[1,2,3,4], Félix Hernández[3,6], Jesús Ávila[3,6], José Luis Lanciego[3,7], Mario Nuvolone[9], Adriano Aguzzi[8], Rosalina Gavín[1,2,3,4,12], Isidro Ferrer[3,5,12] & José Antonio del Río[1,2,3,4,12]✉

The cellular prion protein (PrP^C) plays many roles in the developing and adult brain. In addition, PrP^C binds to several amyloids in oligomeric and prefibrillar forms and may act as a putative receptor of abnormal misfolded protein species. The role of PrP^C in tau seeding and spreading is not known. In the present study, we have inoculated well-characterized sarkosyl-insoluble fractions of sporadic Alzheimer's disease (sAD) into the brain of adult wild-type mice (*Prnp*$^{+/+}$), *Prnp*$^{0/0}$ (ZH3 strain) mice, and mice over-expressing the secreted form of PrP^C lacking their GPI anchor (Tg44 strain). Phospho-tau (ptau) seeding and spreading involving neurons and oligodendrocytes were observed three and six months after inoculation. 3Rtau and 4Rtau deposits from the host tau, as revealed by inoculating *Mapt*$^{0/0}$ mice and by using specific anti-mouse and anti-human tau antibodies suggest modulation of exon 10 splicing of the host mouse *Mapt* gene elicited by exogenous sAD-tau. However, no tau seeding and spreading differences were observed among *Prnp* genotypes. Our results show that PrP^C does not affect tau seeding and spreading in vivo.

Keywords PrP^C, *Prnp*, Tau, *Mapt*, Alzheimer's disease, Seeding, Spreading

Human tauopathies are clinically, neuropathologically, and biochemically distinct neurodegenerative diseases characterized by the deposition of abnormally misfolded and aggregated microtubule-associated protein tau in neurons and glial cells[1–4]. The principal tau deposits comprise 4Rtau, 3Rtau, or 3Rtau + 4Rtau, resulting from the alternative splicing of exon 10 of the tau gene *Mapt*[5]. Alzheimer's disease is a combined 3R + 4R tauopathy and β-amyloidopathy[6–8]; frontotemporal lobar degeneration linked to *MAPT* mutations (FTLD-tau), argyrophilic grain disease (AGD), primary age-related tauopathy (PART), globular glial tauopathy (GGT), progressive supranuclear palsy (PSP), and age-related tau astrogliopathy (ARTAG) are 4R tauopathies and Pick's disease is a 3R tauopathy[3,9–17].

The neuropathology of tauopathies depends on several factors, including the genetic background, selective cellular and regional vulnerability, and progression. One of the mechanisms of disease progression is the

[1]Molecular and Cellular Neurobiotechnology, Institute for Bioengineering of Catalonia (IBEC), Parc Científic de Barcelona, Baldiri and Reixac 15-21, 08028 Barcelona, Spain. [2]Department of Cell Biology, Physiology and Immunology, Faculty of Biology, University of Barcelona, Barcelona, Spain. [3]Cibernet (Network Centre of Biomedical Research of Neurodegenerative Diseases), Institute of Health Carlos III, Madrid, Spain. [4]Institute of Neuroscience, University of Barcelona, Barcelona, Spain. [5]Department of Pathology and Experimental Therapeutics, University of Barcelona, Bellvitge University Hospital-IDIBELL, Hospitalet de Llobregat, Barcelona, Spain. [6]Centro de Biología Molecular 'Severo Ochoa' (CBMSO) CSIC/UAM, Madrid, Spain. [7]Department of Neurosciences, Center for Applied Medical Research (CIMA), Universidad de Navarra, Pamplona, Spain. [8]Amyloidosis Research and Treatment Center, Foundation Scientific Institute Policlinico San Matteo, Department of Molecular Medicine, University of Pavia, Pavia, Italy. [9]Institute of Neuropathology, University of Zurich, Zurich, Switzerland. [10]Present address: Neuroscience Research Institute and Molecular, Cell and Developmental Biology, University of California Santa Barbara, Santa Barbara, CA, USA. [11]These authors contributed equally: Julia Sala-Jarque and Vanessa Gil. [12]These authors jointly supervised this work: Rosalina Gavín, Isidro Ferrer and José Antonio del Río. ✉email: jadelrio@ibecbarcelona.eu

transmission of abnormal proteins from one cell to another, reminiscent of prion transmission[18]. The hypothesis is supported by the capacity to seed an inoculated abnormal protein into the brain of a host and the spreading to connected brain regions[19]. Abnormal tau from tau-enriched brain homogenate fractions from distinct tauopathies has been used as inoculums in several mouse models, thus further validating the capacity of abnormal tau to seed, recruit host tau, transform host tau into an aberrant tau species, and transmit the new abnormal tau to neighboring cells. Mouse hosts include transgenic mice expressing human mutant tau[19–22], mice over-expressing tau[23], and wild type mice[16,24–30].

Several mechanisms are implicated in the uptake of abnormal proteins. One of them is mediated by specific receptors. Focusing on tau, the low-density lipoprotein receptor-related protein 1 (LRP1)[31,32], the cellular prion protein (PrP^C)[33–35], and the lymphocyte-activation gene 3 (LAG3)[36,37] have been described as functional neuronal receptors of tau in experimental models.

PrP^C is a cell surface GPI-anchored protein expressed in several tissues, with high levels expressed in neurons and glial cells[38–41]. The PrP^C central region contains a central hydrophobic domain (HD or HR, aa 110/113–133) and a charged cluster domain (CD, aa 94–110), both involved in binding to distinct oligomeric/fibrillar amyloids, such as prions, β-amyloid and α-synuclein[42–51]. Over-expressed PrP^C binds tau[33–35], and PrP^C mediates the hippocampal synaptic plasticity by soluble tau[52]. However, the putative role of cellular prion protein in tau seeding and spreading in wild-type mice is still unclear.

The present study is designed to assess the role of PrP^C in tau seeding and spreading following the intracerebral inoculation of sarkosyl-insoluble fractions from sAD in mouse models. For this purpose, in addition to wild-type mice (*Prnp*$^{+/+}$), we have used mutant *Prnp* mice over-expressing the GPI truncated form of the cellular prion protein: the "anchorless" GPI$^-$ *Prnp* (Tg44) mouse strain[53] and ZH3 mouse strain lacking *Prnp* mice[54].

Results

Characterization of the tau species used in the study

Western blotting of the sarkosyl-insoluble fractions of sAD cases was processed with the anti-ptau Ser422 (pSer422) antibody. The best profile was obtained in the case of a 65-year-old woman with dementia, showing three bands of around 68, 64, and 60 kDa, together with an upper band of 73 kDa, several bands of about 50 kDa, bands between 30 to 40 kDa, and two lower bands of truncated tau at the C-terminal, one of which was of about 25 kDa; a smear of higher molecular weight-represented large tau aggregates (Fig. 1A). TEM of the same sarkosyl-insoluble fraction revealed the presence of typical paired helical filaments (Fig. 1B). In parallel, we analyzed with TEM the aggregation of the tau K18 fragment in the presence (Hep +) or absence (Hep −) of heparin, to be used as controls in our in vitro experiments. As expected, K18 only forms fibers in the presence of heparin, as revealed in TEM (Fig. 1C,D). Next, we explored the seeding properties of the sarkosyl-insoluble fraction of the sAD patient using the Tau RD P301S Biosensor cell line. Tau K18 (Hep +) (Fig. 1F), sarkosyl-insoluble fractions of P301S transgenic mice (sP301S$^{+/-}$) (Fig. 1I), and the sarkosyl-insoluble fraction of the sAD patient (Fig. 1J) were able to induce the formation of numerous eGFP aggregates in the cytoplasm of the cell line, thereby indicating their seeding properties. In contrast, no or very few eGFP aggregates were seen following incubation with tau K18 (Hep −) (Fig. 1G), and no aggregates were observed with the sarkosyl-insoluble fraction from P301S non-transgenic mice (sP301S$^{-/-}$) (Fig. 1H), and the vehicle (Fig. 1E).

In additional controls, the treatment of the Tau RD P301S Biosensor cell line with (i) monomeric tau Cy5 (Supplementary Fig. S1A–C), (ii) murine or human preformed fibrils of α-synuclein (Supplementary Fig. S1D–E), and (iii) sarkosyl-insoluble brain extracts from multiple system atrophy (MSA) (Supplementary Fig. S1F), and Parkinson's disease (PD) (Supplementary Fig. S1G) were unable to generate intracellular fluorescence aggregates. In contrast, treatments of Tau RD P301S cells with sarkosyl-insoluble fractions from aging-related tau astrogliopathy (ARTAG, a 4R tauopathy) (Supplementary Fig. S1H); Pick's disease (PiD, a 3R tauopathy) (Supplementary Fig. S1I), and globular glial tauopathy (GGT, a 4R tauopathy) (Supplementary Fig. S1J) used in previous studies (Ferrer et al., 2018; Ferrer et al., 2022; Ferrer et al., 2020) render intracellular fluorescence aggregates indicating tau seeding properties.

Characterization of PrP^C expression in mouse strains used in the study

The expression of PrP^C was assessed in wild-type (*Prnp*$^{+/+}$), ZH3 *Prnp*$^{0/0}$, and GPI$^-$ *Prnp* mouse hippocampus using Western blot and immunohistochemistry using the 6H4 anti-PrP^C antibody (Fig. 2, Supplementary Fig. S2). In parallel, PrP^C was absent in ZH3 *Prnp*$^{0/0}$ mouse extracts; a band of around 25kDa was obtained with GPI$^-$ *Prnp* brain extracts, as previously described[53]. In contrast, three bands were observed in (*Prnp*$^{+/+}$) brain extracts (Fig. 2A). Next, sections from wild-type (Fig. 2B), ZH3 *Prnp*$^{0/0}$ (Fig. 2C), and GPI$^-$ *Prnp* (Fig. 2D) mice were processed for PrP^C immunohistochemistry. PrP^C immunostaining was intense in *Prnp*$^{+/+}$, particularly in the CA1 region, and lesser in the dentate gyrus (Fig. 2B). In contrast, the ZH3 *Prnp*$^{0/0}$ (Fig. 2C) and GPI$^-$ *Prnp* (Fig. 2D) hippocampus showed a pale 6H4 labeling consistent with non-specific background. Lack of PrP^C immunostaining was corroborated in hippocampal sections from *Nestin-cre Prnp*$^{flox/flox}$ mice compared to *Prnp*$^{flox/flox}$ lacking cre expression (Fig. 2E–F).

The absence of PrP^C expression or the expression of anchorless PrP^C does not impair endogenous tau aggregation after sAD inoculation

ZH3 *Prnp*$^{0/0}$, GPI$^-$ *Prnp,* and wild-type (*Prnp*$^{+/+}$) mice aged 4–5 months were inoculated with sAD in the cortex/corpus callosum and hippocampus and analyzed 3 and 6 months later (Fig. 3). As controls, 4 wild-type mice were inoculated either with PBS 0.1M (n = 2), sarkosyl fractions of a non-AD patients (n = 2) and processed 3 months post-inoculation (Supplementary Fig. S3). Numerous AT8-positive deposits were found in sAD inoculated mice irrespective of their genotype and post-inoculation time (Fig. 3) in contrast to PBS 0.1M or non-AD sarkosyl

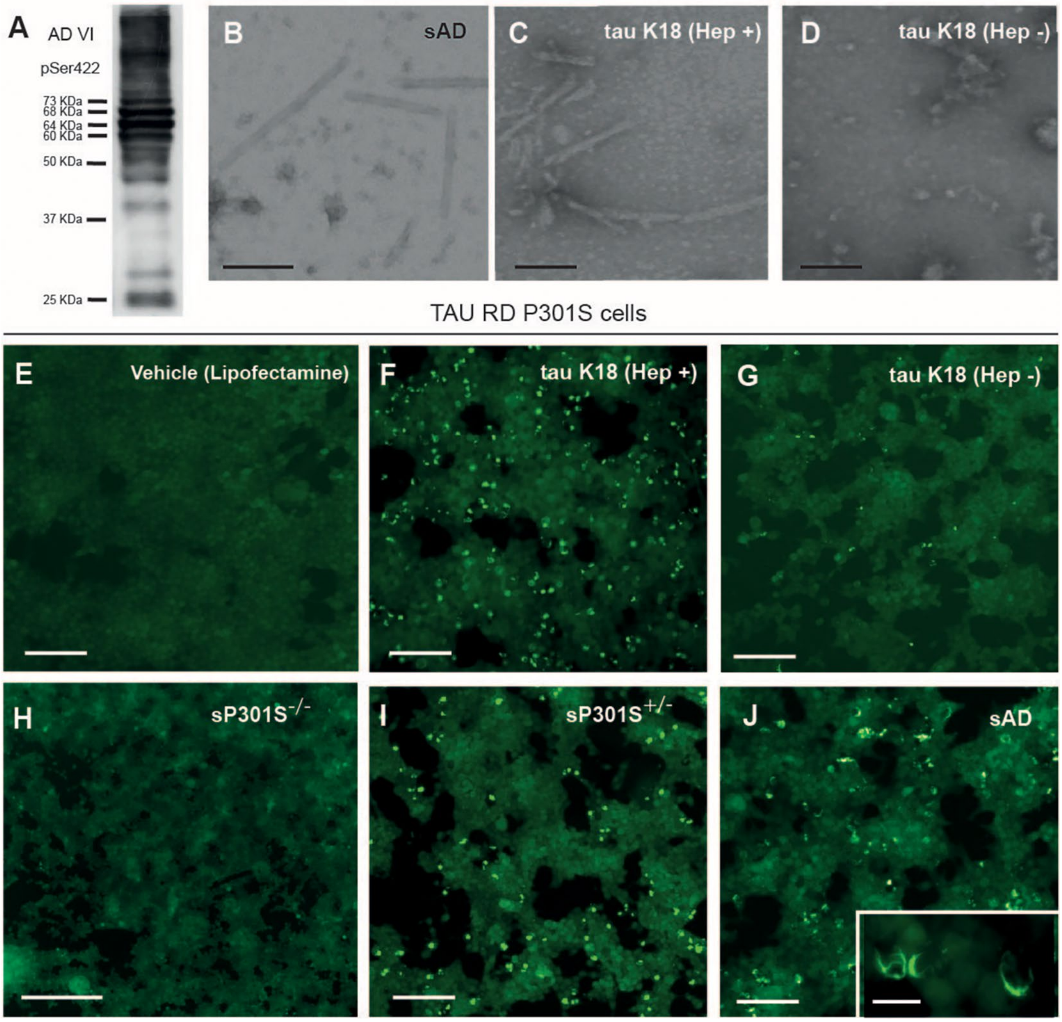

Fig. 1. Characterization of the sarkosyl-insoluble fraction. (**A**) Western blot of the selected sarkosyl-insoluble fraction from the AD patient (sAD) immunoblotted using the pSer422 antibody showing three bands of about 68, 64, and 60 kDa, together with an upper band of 73 kDa, several bands of about 50 kDa, bands between 30 and 40 kDa, and two lower bands of truncated tau at the C-terminal. (**B–D**) TEM negative staining of the sAD sarkosyl-insoluble fractions (**B**) and tau K18 fragment after their fibrillation with (**C**) or without heparin (**D**). (**E–J**) seed competency experiments using the Tau RD P301S cell line, including vehicle (**E**), fibrillar tau K18 (**F**), non-fibrillated tau K18 (**G**), sarkosyl-insoluble fraction from a P301S non-transgenic mouse (**H**), P301S transgenic mouse (**I**), and sAD (**J**). Notice the presence of fluorescence aggregates in (**F**), (**I**), and (**J**) in contrast to vehicle, non-fibrillated tau K18, and sP301S$^{-/-}$ (wild-type) extracts. Scale bars: A–C = 0.5 µm, E–J = 200 µm; insert in J = 50 µm.

fractions (Supplementary Fig. S3). AT8-positive inclusions of different morphologies (pre-tangles, threads, and granular, but not neurofibrillary tangles) were observed mainly in neurons (Fig. 3G), and oligodendrocytes (Fig. 3K–M) immunolabeled with AT8 and MC-1 (Fig. 3E–F) antibodies, but not in astrocytes (Fig. 3HI). Numerous AT8-positive ptau deposits were observed in axonal tracts (Fig. 3J). Ptau inclusions were also positive with X34, a highly fluorescent derivative of Congo red, used for a sensitive detection of pathological amyloid structures (Supplementary Fig. S4). A few labeled neurons were observed in the contralateral neocortex and hippocampus (Fig. 3B–C). Mice treated with AD-derived sarkosyl-insoluble fractions showed double-labeled cells containing AT8-positive deposits and intense P62 labeling (Supplementary Fig. S5), thus suggesting altered proteostasis in AT8-immunoreactive cells after sAD inoculation. No differences in the ptau deposits and their cellular localization were observed when all *Prnp* genotypes were compared at the analyzed time points.

A comparison of ptau localization and corpus callosum extension in *Prnp*$^{+/+}$, ZH3 *Prnp*$^{0/0}$, and GPI^{-} *Prnp* inoculated mice at the age of 4–5 months and killed three months and six months after inoculation is shown in Fig. 4. At three months after inoculation, AT-8-immunoreactive deposits were seen in the ipsilateral corpus callosum, crossing the midline and extending to the medial part of the contralateral corpus callosum in sections obtained at the level of the site of the injection (Fig. 4A–C). AT8 immunostaining in the corpus callosum was more intense at six months post-inoculation compared to 3 months. Still, the distribution of the

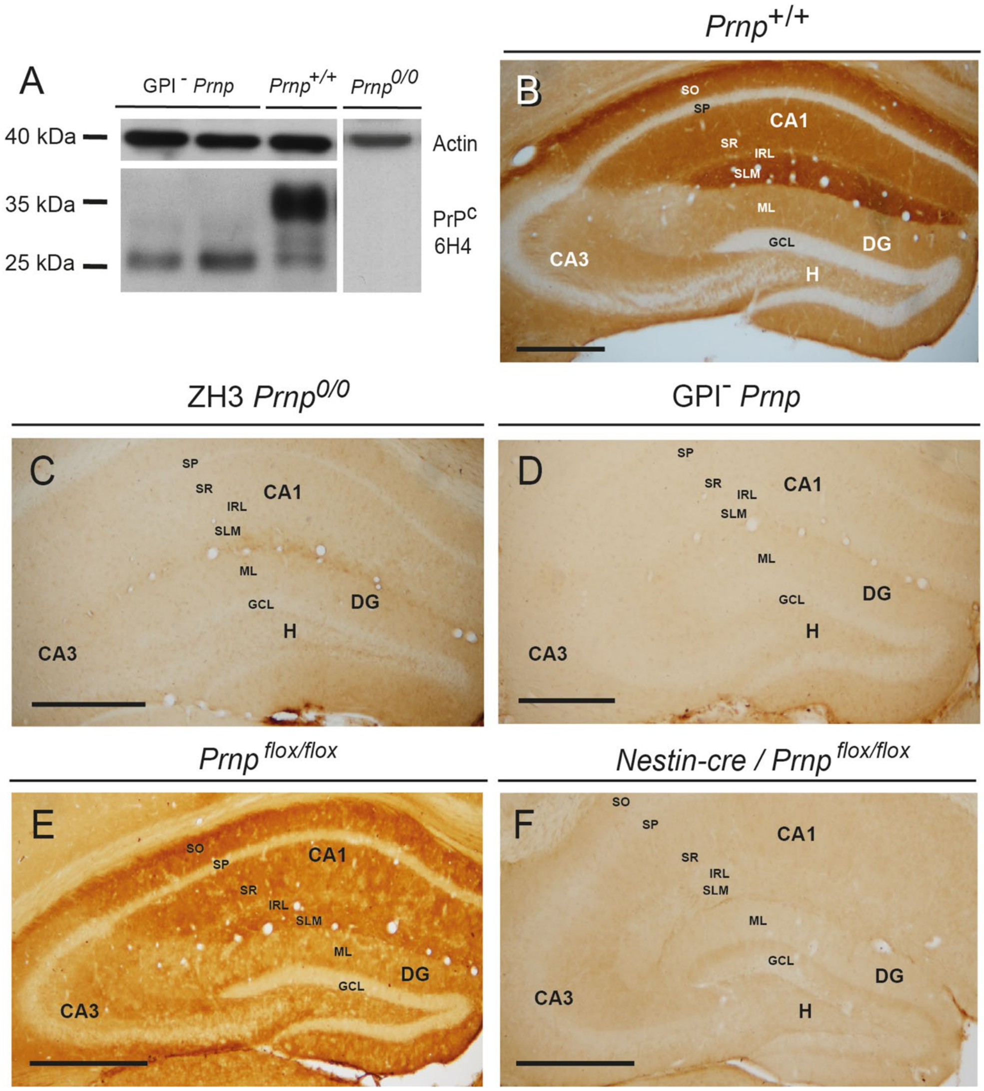

Fig. 2. PrP^C expression in *Prnp*$^{+/+}$; ZH3 *Prnp*$^{0/0}$, and GPI$^-$ *Prnp* mice. (**A**) Western blot of brain extracts from the three genotypes immunoblotted using 6H4 against PrP^C and actin as a protein loading control. Note the absence of PrP^C labeling in ZH3 *Prnp*$^{0/0}$, the unique lower band in anchorless PrP^C mice, and the triple band in wild-type mice *Prnp*$^{+/+}$. (**B–D**) Low-power photomicrographs illustrating coronal hippocampal sections immunostained with anti-PrP^C antibodies. Intense immunolabelling is seen in *Prnp*$^{+/+}$ hippocampus, especially in the CA1 region (**B**). In contrast, a pale uniform background (negative immunostaining) is observed in the ZH3 *Prnp*$^{0/0}$ and GPI$^-$ *Prnp* hippocampus (**C**–**D**). (**E–F**) 6H4 immunostaining in the *Prnp*$^{flox/flox}$ (**E**) *Nestin-cre* / *Prnp*$^{flox/flox}$ (**F**). Notice the absence of PrP^C labelling in *Nestin-cre*/*Prnp*$^{flox/flox}$ hippocampus. CA1–CA3: *cornus ammonis* 1 and 3; DG: Dentate gyrus; H: Hilus; SO: *stratum oriens;* SP: *stratum pyramidale;* SR: *stratum radiatum*; IRL: interphase *radiatum-lacunosum moleculare*; SLM: *stratum lacunosum-moleculare*; ML: molecular layer; GCL: granule cell later. Scale bars: B–F = 500 µm.

AT8-positive deposits in the corpus callosum was the same as at three months (Fig. 4D–F). Similar localization and distribution of AT8-immunoreactive deposits were observed in *Prnp*$^{+/+}$, GPI$^-$ *Prnp*$^{0/0}$, and ZH3 *Prnp*$^{0/0}$ mice after injection of AD-derived sarkosyl-insoluble fractions. After quantification of the area occupied by the AT8-positive ptau (Fig. 4G), no significative statistical differences were observed between phenotypes and post-inoculation time although an increased presence was observed between 3- and 6-months post-inoculation as above indicated: (3 months post- inoculation: ZH3 *Prnp*$^{0/0}$ = 9606.71 ± 624.17 *Prnp*$^{+/+}$ = 10,512.066 ± 482.81; GPI$^-$*Prnp*$^{0/0}$ = 8784.19 ± 1171.99. 6 months post-inoculation: ZH3 *Prnp*$^{0/0}$ = 13,054.37 ± 1361.18; *Prnp*$^{+/+}$ = 14,070.38 ± 1156.85; GPI$^-$*Prnp*$^{0/0}$ = 13,394.42 ± 1774.22 (all data is represented as µm^2 (mean ± s.e.m.) of AT8-positive deposits/146,850 µm^2 photomicrographic field, see Methods for details, and Supplementary Fig. S6 for an example of this analysis in a ZH3 *Prnp*$^{0/0}$ photomicrograph).

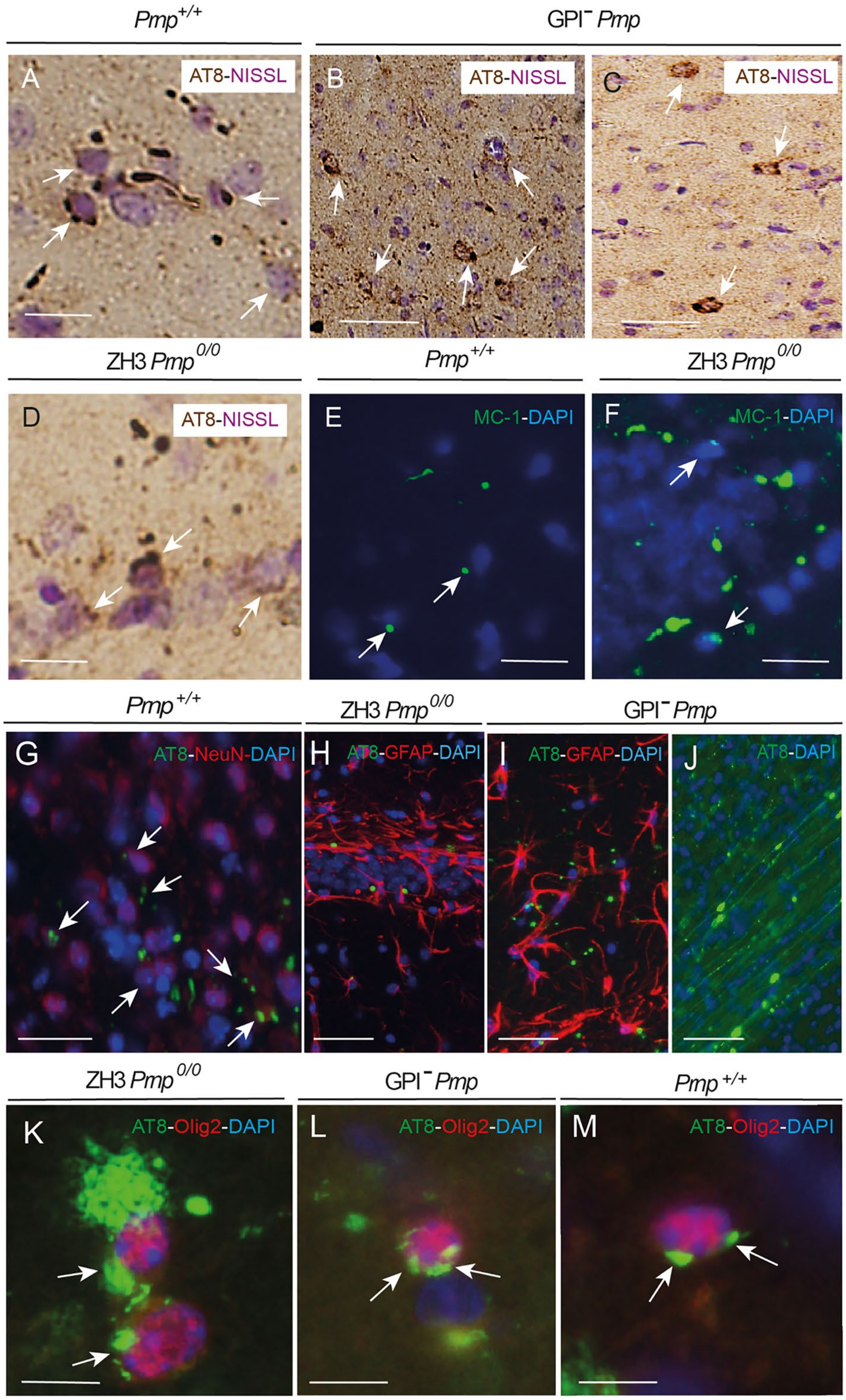

Fig. 3. AT8- and MC1-positive deposits in *Prnp*$^{+/+}$; ZH3 *Prnp*$^{0/0}$, and GPI^{-} *Prnp* mice. Immunostaining after sAD inoculation at three months (**B**–**C**) and six months (**A**, **E**–**M**) post-inoculation (**A**) AT8-positive grains (arrows) and threads in the SLM of CA1. The section was Nissl counterstained. (**B**–**C**) AT8-positive neurons (arrows in B and C) are seen in the retrosplenial cortex (ipsilateral (B) and contralateral (C)) after sAD inoculation. Sections were Nissl counterstained. (**D**) Example of AT8-positive grains (arrows) and threads in the SLM of CA1 of ZH3 *Prnp*$^{0/0}$. The section was Nissl counterstained. (**E**–**F**) MC-1-positive threads and grains (arrows) in the lower cortical layers after sAD inoculation (**E**) and in the hippocampus of wild-type and ZH3 *Prnp*$^{0/0}$ mice. Sections were counterstained with DAPI. (**G**) Double-immunofluorescence with NeuN (red) and AT8 (green) in lower cortical layers. Note the presence of some ptau deposits in NeuN-positive neurons (arrows). The section was counterstained with DAPI (**H**–**I**) Absence of double-labeled GFAP (red) and AT8 (green) cells in the CA1 region of inoculated mice. ZH3 *Prnp*$^{0/0}$ (**H**) and GPI^{-} *Prnp* (**I**). (**J**) AT8 immunofluorescence (green) of axonal tracts in the white matter of the corpus callosum (arrows) of inoculated GPI^{-} *Prnp* mouse. The section was counterstained with DAPI. (**K**–**M**) Double-immunofluorescence showing Olig2-positive oligodendrocytes (red) containing AT8-positive inclusions (green and arrows) in the white matter of ZH3 *Prnp*$^{0/0}$ (K), GPI^{-} *Prnp* (L), and wild-type (M)). Sections were counterstained with DAPI. Scale bars: A–D = 50 µm; E–J = 100 µm; K–M = 50 µm.

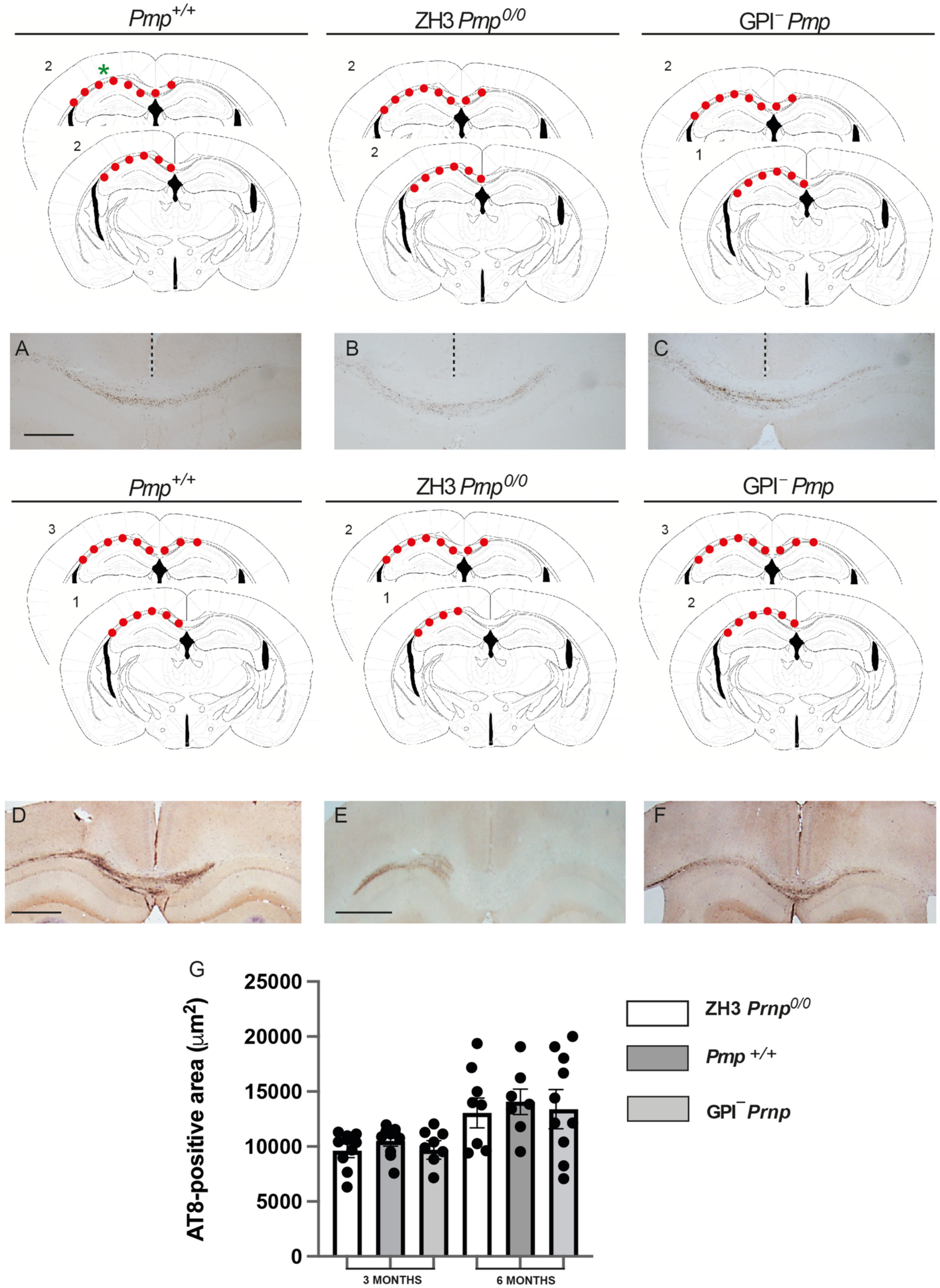

Fig. 4. AT8-positive deposits in the white matter after 3 and 6 months post-sAD inoculation. For each genotype, two schemes are included. In each scheme, the distribution of AT8-positive deposits is illustrated in red dots. A green asterisk indicates the injection site (**A**); the number of inoculated mice showing the distribution stated in the scheme is displayed in the upper left corner. (**A–C**) Photomicrographs illustrating the distribution of AT8-positive deposits in the three genotypes three months after sAD inoculation. (**D–F**) Photomicrographs show AT8-positive deposits in the three genotypes six months after sAD inoculation. The inter-hemispheric fissure is labeled with a dashed line in (**A**–**C**). Note the increase in the labeling between 3 and 6 months post-sAD inoculation. The distribution of ptau deposits is similar in the three genotypes and at the two post-inoculation times. (**G**) Histogram illustrating the results of the quantification of the area occupied by AT8-positive deposits for each of the genotypes and ages (3 or 6 months post-sAD) analyzed. Each point represents the value obtained from one section. See Methods for details and Supplementary Fig. S6 for an example. Values are represented as the mean and s.e.m.. Scale bars: A–C = 250 µm, D = 500 µm; E and F = 500 µm.

AD sarkosyl-insoluble fraction inoculation triggers mouse ptau recruitment and 3Rtau + 4Rtau expression in the host

Inoculation of sAD sarkosyl-insoluble fractions produced seeding and spreading in wild-type mice (*Prnp*$^{+/+}$) but not in inoculated *Mapt*$^{0/0}$ mice (Fig. 5A,B), thus supporting the endogenous origin of AT8-positive ptau deposits in inoculated animals. The endogenous origin of ptau in inoculated mice was corroborated by immunohistochemistry using Tau13 (human-specific) (Fig. 5C–E, Supplementary Fig. S7A-F) and T49 (mouse-specific) and anti-tau antibodies (Fig. 5F–H, Supplementary Fig. S7G-L). Double-labeling immunostaining showed co-localization of pSer422-positive aggregates and T49 but not pSer422-positive ptau aggregates and Tau13 (Fig. 5C–H, Supplementary Fig. S7A–F).

Finally, we aimed to determine whether the observed ptau inclusions contained 3R and 4Rtau isoforms using specific antibodies. Double-labeling immunofluorescence demonstrated the presence of 3R and 4Rtau isoforms in pSer422-positive aggregates (Fig. 5I–S, Supplementary Fig. S8), thus suggesting impaired gene regulation in cells containing abnormal ptau deposits.

Discussion

PrP^C involves many functions in the developing and adult brain[55–57]. PrP^C is also involved in neurodegeneration, interacting with several amyloid proteins, thus participating in the pathogenesis of several neurodegenerative diseases with abnormal protein aggregates[42–47,49–51,58,59]. PrP^C has been implicated in the pathological protein aggregates uptake and toxic signaling[58]. In this line, we showed the involvement of the cellular prion protein in α-synuclein transport in neurons[48] in parallel to others studies reviewed in[51].

In the present study, after characterization of the sAD homogenates used for inoculation in mice and validation of their suitability as seeding products in Biosensor cells, we have tested the hypothesis that PrP^C might play a role in tau seeding and spreading in vivo. As previously reported, we have observed ptau seeding and spreading of inoculated sAD-tau in wild-type mice[16,23]. In addition to neurons, oligodendrocytes are targets of ptau seeding and ptau propagation[60] irrespective of PrP^C expression levels and its location (extracellular *vs* membrane-linked).

Another relevant point has been the observation that 3Rtau and 4Rtau deposits are produced by the host (as revealed with specific anti-mouse and anti-human tau antibodies) following the intracerebral inoculation of sAD (3R + 4Rtau). Similar observations were observed in other paradigms[16,23,60,61]. Since mice express predominant 4Rtau in the mature brain, the appearance of 3R and 4R tau suggests that exogenous ptau modulates *Mapt* splicing in the host. A similar shift between 4 and 3Rtau has been described near the ischemic core following middle cerebral occlusion[62] Similarly, human tau (4R isoform) packaged into the recombinant AAV serotype 9 inoculated in the rhesus monkey hippocampus, resulted in 3Rtau and 4Rtau accumulation, tau phosphorylation, and propagation two or three months after injection[62]. However, other studies have not observed a change in the expression of tau isoforms in inoculated mice models[24,29,63–65]. These findings support the notion that different tau strains produce distinct patterns of neuronal tau deposition and seeding and also that tau seeding depends on the host tau[30,60,66,67].

Regarding our main objective, we have used two *Prnp* mouse transgenic mice, *Prnp* mice over-expressing the GPI truncated form of prion protein: the "anchorless" GPI$^-$ *Prnp* and ZH3 *Prnp*$^{0/0}$, to assess whether PrP^C is needed for tau seeding and spreading in vivo. Our results prove that it is not for ptau since both processes occurs in all *Prnp* genotypes. However, we cannot rule out a minor role of PrP^C that could be masked to the relevant function of LRP1[31,32] or LAG3[37], as well as other mechanisms in these processes[68]. In fact, extracellular amyloid proteins mainly prefibrilar or fibrillar treatments can render kinase (e.g., p38, ERK1/2) activation as well other intracellular effects (NADPH activation and ROS generation) in absence of PrP^C[69–71] that might lead endogenous mouse ptau generation (e.g., see[72,73] for reviews). Another scenario, might be related to the fact that although the physical interaction of PrP^C mainly with oligomers of Aβ, α-synuclein, tau, and TDP43 has already been described (i.e.,[45,48,50,58,59]), some studies reported that PrP^C cannot bind to oligomeric species of α-synuclein[74] or Aβ[75], or that their effects in neuronal activity or survival are not linked to PrP^C[76,77] in contrast to ([33,78]). In fact, these divergences could be linked to the preparation of the samples since it has been described that fibrils and globular oligomers bind only weakly to PrP^C and mediate toxicity in a PrP^C-independent manner[78] (see also[58] for additional comments). However, we believe that our results using sarkosyl-insoluble fractions of AD containing tau seeding properties points a null or minor role of PrP^C in seeding and spreading of these sAD fractions in parallel to some of the previously commented studies, in contrast to their relevant role in the progression of inoculated mice with α-synuclein prefibrils[48].

Methods

Mouse strains

Adult ZH3 *Prnp*$^{0/0}$ mouse line was generated by A. Aguzzi (Switzerland)[54]. Mice over-expressing the secreted form of PrP^C lacking their GPI anchor (GPI$^-$ *Prnp* (Tg44 strain) mice were kindly provided by Vincent Beringue, INRA UR892, Virologie Immunologie Moléculaires, Paris, France)[53]. Mice lacking tau (*Mapt*$^{0/079}$) were kindly provided by Jesús Ávila, CBM-UAM, Madrid). P301S (PS19) transgenic mice[80] that over-express the human mutation of tau under the cellular prion protein promoter[81] were obtained from Jackson Laboratories ref: 008169. Nestin-cre/*Prnp*$^{flox/flox}$ mice were generated in our laboratory by crossing *Prnp*$^{\text{flox/flox}}$[82] and Nestin-cre[83]. A total of 48 adult (2–5 months old) male mice included *Prnp*$^{+/+}$ (n = 15), *Prnp*$^{0/0}$ (n = 8), GPI$^-$ *Prnp* (n = 11), *Mapt*$^{0/0}$ (n = 3), *Prnp*$^{flox/flox}$ (n = 2) and Nestin-cre/*Prnp*$^{flox/flox}$ (n = 5). In addition, 4 mice of our P301S colony (12 months of age) were used to obtain sarkosyl-insoluble brain fractions: P301S$^{+/-}$ (n = 2); P301S$^{-/-}$ (n = 2). All the animals were kept in the animal facility at the Faculty of Pharmacy, University of Barcelona, under controlled environmental conditions and were provided food and drink ad libitum. All experiments were performed under the guidelines and protocols of the Ethical Committee for Animal Experimentation (CEEA) of the University of Barcelona;

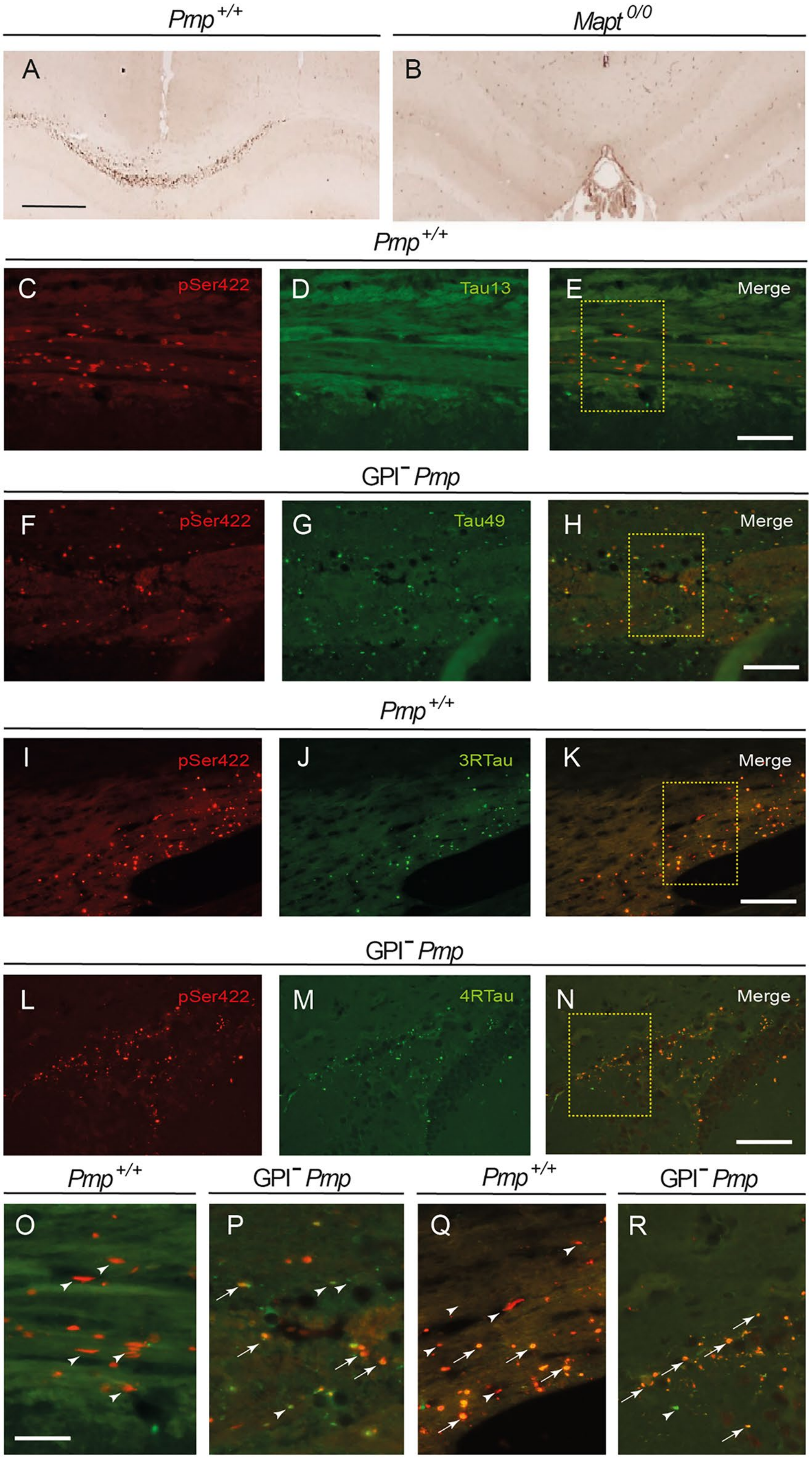

Fig. 5. Characterization of ptau deposits. (**A**) After sAD inoculation immunostained with the AT8 antibody, a wild-type mouse showed AT8-positive deposits along the corpus callosum. (**B**) *Mapt*$^{0/0}$ mouse three months post-sAD inoculation shows negative AT8 immunostaining. (**C–E**) Double-labeling immunofluorescence with pSer422 (**C**) and Tau13 (anti-human tau) (**D**) showing lack of co-localization. (**F–H**) Double-labeling immunofluorescence with pSer422 (**F**) and Tau 49 (anti-mouse tau) (**G**) shows co-localization of the antibodies, thus indicating the mouse origin of tau in ptau deposits. (**I–O**) Double-labeling immunofluorescence using pSer422 (**I**,**M**) and 3Rtau (**J**) and 4Rtau (N) specific antibodies show co-localization of pSer422 and 3Rtau, and pSer422 and 4Rtau in deposits. (**P–S**) High magnifications of the above-mentioned results boxed in (**E**), (**H**), (**L**) and (**O**). In the Figure, double labelled cells are indicated as arrows and arrowheads point to non-double labelled ptau deposits. The post-inoculation time in C–S was 6 months. The genotype of each inoculated mice is illustrated. Scale bars: A and B = 500µm, C–O = 100µm, P–S = 75µm.

the protocol for the use of animals in this study was reviewed and approved by the CEEA of the University of Barcelona (CEEA approval #276/16 and #141/15), and comply with the guidelines and regulations of ARRIVE essential 10 guidelines 2.0[84].

Human brain samples

Brain samples were obtained from the Institute of Neuropathology Brain Bank, Bellvitge University Hospital, following the guidelines of the Spanish legislation on this matter (Real Decreto Biobancos 1716/2011) and the approval of the local ethics committee of Bellvitge University Hospital (Hospitalet de Llobregat, Barcelona, Spain). At the time of the autopsy, one hemisphere was fixed in paraformaldehyde. The other hemisphere was cut into coronal Sects. 1 mm thick, and selected brain regions were dissected, immediately frozen at − 80 °C, put on labeled plastic bags, and stored at − 80 °C until use; the rest of the coronal sections were frozen and stored at −80 °C following standard protocols[85].

Sarkosyl-insoluble fractions from the frontal cortex (area 8) of ten patients with sAD were characterized. After the clinical, neuropathological, and biochemical study, we selected samples from a 56-year-old female with non-familiar dementia; the genetic study of *APP*, *PSEN1*, and *PSEN2* revealed no mutations and duplications. The clinical record revealed no infectious diseases, seizures, vascular diseases, and no prolonged agonal state; at post-mortem, the pH of the brain was 6.8. The neuropathological examination categorized sAD as NFT Braak stage VI, Thal phase 4, and CERAD 3; concomitant pathologies including 4Rtaupathies (argyrophilic grain disease: AGD, aging-related tau astrogliopathy: ARTAG), Lewy body disease, limbic-predominant TDP-43 encephalopathy, and hippocampal sclerosis were absent.

In addition, stored sarkosyl-insoluble fractions from AGD, ARTAG and globular glial tauopathy (GGT), healthy non-neurodegenerative cases (already used in previous studies:[16,23,27]), and extracts from post-mortem brain samples of Parkinson's disease (PD) and multiple system atrophy (MSA) (Navarra biobank) were employed for comparison in specific experiments.

Sarkosyl-insoluble fraction preparation

Brain tissue was weighed and then homogenized using a Dounce homogenizer in 10 volumes of fresh homogenization buffer (0.8M NaCl, 1mM EGTA, 10% sucrose, 0.01M $Na_2H_2P_2O_7$, 0.1M NaF, 2 mM Na_3VO_4, 0.025M β-glycerolphosphate, 0.01M Tris–HCl pH 7.4) containing protease inhibitors (Roche, Switzerland). After centrifugation at 16,000 rpm for 22 min at 4 °C, the supernatant was reserved (SN1). The pellet was re-suspended in 5 volumes of homogenization buffer and centrifuged at 14,000 rpm for 22 min at 4 °C. The resulting supernatant (SN2) was then combined with the SN1, and the mixture (SN1 + SN2) was incubated with 0.1% N-lauroyl sarcosinate (sarkosyl; Sigma-Aldrich) and placed on a rotating shaker for one h at room temperature. The mixture was centrifuged at 35,000 rpm for 63 min at 4 °C. The resultant supernatant was discarded, and the remaining pellet (sarkosyl-insoluble fraction) was washed and re-suspended in 50 mM Tris–HCl, pH 7.4 (200 µl/g starting material). Finally, 100 µl aliquots were stored at − 80 °C until use. Protein concentrations were determined using the Pierce™ BCA assay kit (Sigma-Aldrich), and equal amounts of protein were analyzed with western blot.

Biochemical analysis

Following dodecyl sulfate–polyacrylamide gel electrophoresis (SDS-PAGE) and Western blotting samples were characterized. Protein extracts were boiled at 100 °C for 10 min, followed by SDS-PAGE electrophoresis, and they were then electro-transferred to nitrocellulose membranes for 1 h at 4 °C. Membranes were then blocked with 5% fat milk in 0.1M Tris-buffered saline (pH 7.4) for 1 h and incubated overnight in a 0.5% blocking solution containing the primary antibodies. After incubation with peroxidase-tagged secondary antibodies (at a dilution of 1:2,000, Sigma-Aldrich), the membranes were revealed with an ECL-plus chemiluminescence Western blot kit (Amersham-Pharmacia Biotech).

Tau RD P301S Biosensor cell line experiments

The Tau RD P301S Tau Biosensor (ATCC® CRL-3275™) was purchased from ATCC. Cells were grown in the maintenance medium Dulbecco's Modified Eagle Medium (DMEM; Thermo Fischer Scientific), supplemented with 10% fetal bovine serum (FBS; Thermo Fischer Scientific), 1% GlutaMax (Gibco), and 1% Penicillin/Streptomycin (Thermo Fischer Scientific) in 75 cm^2 culture flasks (Nunc). Cells were maintained at 37 °C and 5% CO_2 in a humidified incubator and passaged every three days when confluent. Tau Biosensor cells were plated in 96-well poly-D-lysine (Sigma-Aldrich) (0.1 mg/ml) coated plates at a density of 35,000 cells/well in the maintenance medium (total volume 130 µl) and cultured at 37 °C in a 5% CO_2 incubator overnight. The transduction mixture was prepared following the manufacturer's protocol. Briefly, 1.5 µl of the sample was combined with 8.5 µl of Opti-MEM medium (Thermo Fischer Scientific). A mixture of 1.25 µl Lipofectamine-2000™ reagent (Thermo Fischer Scientific) and 8.75 µl Opti-MEM was added to the sample mixture to a final volume of 20µl and incubated for 1 h at room temperature. Mixtures with empty liposomes were included as negative controls. Tau Biosensor maintenance medium was gently removed and replaced with 130 µl of pre-warmed Opti-MEM before 20 µl the transduction mixture was added to the cells. Twenty-four hours later, cells were washed once with pre-warmed 0.1M PBS and fixed with 4% phosphate-buffered paraformaldehyde (PFA) for 15 min at room temperature. Next, PFA was removed, and cells were washed thrice, 5 min each, with 300 µl of 0.1M PBS. Finally, 300 µl 0.1M PBS with 0.02% NaN_3 was placed in each well; the plate was sealed with Parafilm™ and kept at 4 °C until analysis. The following samples were analyzed: fibrillated and monomeric tau K18 (that encompasses the four microtubule-binding repeats (R1-R4) of the tau protein and is one of the minimal sequences necessary for tau aggregation) at a final concentration of 0.01µM (Bio-techno (ref: SP-496-100)); human and murine α-synuclein pre-formed fibrils at 0.1 µg/µl (a gift from Masato Hasegawa, Tokyo Metropolitan Institute of Medical Science, Japan);

monomeric tau Cy5 at a final concentration of 100nM (kindly provided by Jesús Ávila, CBM-UAM, Madrid). Sarkosyl-insoluble fractions of P301S$^{+/-}$ and P301S$^{-/-}$ (wild-type) mice were used at a final concentration of 0.003 µg/µl. Sarkosyl-insoluble fractions from human brains were used at a final concentration of 0.003 µg/µl.

Negative electron microscopy staining

For transmission electron microscopy (TEM) experiments, tau samples were fixed to carbon-forward-coated copper grids and negatively stained with buffered 1% uranyl acetate (pH 7.4). The samples were placed in silica-based desiccant for at least two hours and examined with a Jeol JEM-1010 transmission electron microscope.

Mouse tissue homogenization and preparation

Mouse brain tissue of the different strains was weighed and diluted in 1 ml 0.1M PBS supplemented with protease inhibitors (Roche, Switzerland) per 20 mg of tissue. The sample was homogenized for 10 min using a Polytron™. Fifty µl aliquots were stored at − 80 °C until use. Protein concentrations were determined using a BCA assay, and equal amounts of protein were analyzed with western blot.

Stereotaxic surgery

Mice were deeply anesthetized with isoflurane and placed in a stereotaxic apparatus (Kopf Instruments, ref: 963, USA). Unilateral stereotaxic injections were made into the right hippocampus (AP: 1.4 mm from Bregma; LM: 1.5 mm). 2.5 µl of sarkosyl extract dissolved in 100mM Tris-HCl was inoculated using a Hamilton syringe into the upper corpus callosum/cortex at DV of 1 mm[86]. Following the injection, the needle was kept in place for an additional 3 min. The surgical area was cleaned with sterile saline, and the incision was sutured. Mice were monitored until recovery from anesthesia and were checked regularly following surgery.

Primary antibodies used in the study

The following primary antibodies were used: monoclonal mouse AT8 against pSer202 and pThr205 residues of ptau (1:50 dilution) (Thermo Fischer Scientific, catalog MN1020), polyclonal rabbit anti-tau-phosphoSer422 (pSer422) (1:75 dilution) (Life Technologies, catalog 44-764G), monoclonal mouse anti-PrP^{C} (6H4 clone) (1:1000 dilution) (Thermo Fischer Scientific, catalog 01-010), human tau-specific antibodies Tau13 (1:200 dilution) (Biolegend, catalog no 835201), murine tau-specific antibody T49 (1:200 dilution) (Merck Millipore, catalog no MABN827), and monoclonal mouse MC-1 anti-tau (a gift of Prof. Peter Davis[87]). Tau isoforms 3R and 4R were assessed using monoclonal mouse antibodies RD3 (clone 8E6/C11) (1:50 dilution) and RD4 (clone 1E1/A6) (1:50 dilution) (Merck Millipore). Other antibodies were polyclonal rabbit anti-P62/SQSTM1 (1:100 dilution) (Progen, ref GP62-C), monoclonal mouse anti-actin (1:1,000 dilution) (Millipore, catalog MAB1501), monoclonal mouse anti-TUJ1 (neuron-specific class III β-tubulin) (1:500 dilution) (BioLegend, catalog 801201).

Tissue processing of sarkosyl-inoculated mice

After 3 (C57BL/6J (n = 10), *MAPT*$^{0/0}$ (n = 3), ZH3-*Prnp*$^{0/0}$ (n = 5), GPI^{-} *Prnp* (n = 5)) and 6 (C57BL/6J (n = 5), ZH3-*Prnp*$^{0/0}$ (n = 3), GPI^{-} *Prnp* (n = 6)) months post-injection, mice were processed for neuropathological study. After deep anesthesia with isoflurane, mice were transcardially perfused with phosphate-buffered 4% PFA (pH 7.3) using a peristaltic infusion pump. The brain was dissected and post-fixed overnight in the same fixative. Post-fixed brains were rinsed in 0.1M PBS and stored in 70% ethanol at 4 °C until paraffin inclusion. Following paraffin embedding, 10 µm thick coronal sections were obtained and mounted on gelatinized glass slides. For immunohistochemistry, paraffin sections were de-waxed in xylene for 20 min, washed in ethanol, and rinsed in miliQ H_2O. Selected de-waxed sections containing the dorsal hippocampus were treated with DakoTarget retrieval solution (pH 9) (Dako, Denmark) at 95 C in a Dako PT Link to retrieve protein antigenicity. After washing in 0.1M Tris–HCl pH 7.6, sections were rinsed in 0.1M PBS; endogenous peroxidase activity was blocked by incubation in 2% H_2O_2 and 10% methanol in 0.1M PBS. After rinsing, sections were incubated in 0.1M PBS containing 0.2% gelatin, 10% fetal bovine serum (FBS), 0.2% glycine, and 0.1% Triton X-100 for 1 h at room temperature. Afterward, the sections were incubated with primary antibodies (all primary antibodies were diluted in 5% FBS, 0.1% Triton X-100, and 0.02% NaN_3 in 0.1M PBS) overnight at 4 °C. For bright-field visualization, tissue sections were then rinsed in 0.1M PBS and incubated for 2 h at room temperature with species-specific biotinylated secondary antibody (1:200 dilution) (Vector Laboratories) in 0.1M PBS, 5% FBS, 0.1% Triton X-100. Sections were incubated with an avidin–biotin-peroxidase complex (ABC) kit following the manufacturer's instructions (Vector Laboratories). Peroxidase activity was developed with 0.03% 3–3'-diaminobenzidine (DAB) and 0.01% H_2O_2. For fluorescence staining, sections were rinsed in 0.1M PBS and incubated with species-specific secondary antibodies, Alexa Fluor-488 or -568 (1:300 dilution) (Life Technologies), for 2 h at room temperature. Then, sections were incubated with 1 µg/ml DAPI (Thermo Fischer Scientific) diluted in 0.1M PBS for 10 min at room temperature, rinsed with 0.1M PBS, and mounted in Mowiol™ (Sigma-Aldrich). Sections were photo-documented using an Olympus BX61 microscope with a cooled digital DP72L camera. As an internal immunohistochemical control for immunohistochemistry, 25 µm thick cryostat sections from the frontal cortex (area 8/9) of AD samples (Braak stage VI) were processed in parallel. For quantification to analyze the degree of ptau seeding after the sAD inoculations, photographs were taken using the 20X objective of areas close to the injection site in the white matter. The images were processed using the ImageJ™ software. For this, the photographed region for each case covered an area of 146,850 µm^2 at a resolution of 1360 × 1024 pixels. Under these conditions, each pixel of the image corresponds to an area of 0.1054 µm^2. The images processed at 16 bits were analyzed to determine the AT8-positive area using an inverted lut and threshold, and subsequently, the occupied area was calculated using the *Particle Analysis* plugin of ImageJ™. A minimum of 2–3 images from each case presented in Fig. 4 were processed. The results were processed using the statistical program GraphPad

Prism 10.0.1.218 (ID: 97F7835C03E), and a non-parametric ANOVA Dunn's multiple comparisons analysis was performed.

Data availability

The data supporting the conclusions of this article will be made available by the corresponding author upon request, without undue reservation.

Received: 30 March 2024; Accepted: 4 September 2024
Published online: 16 September 2024

References

1. Shi, Y. *et al.* Structure-based classification of tauopathies. *Nature* **598**, 359–363. https://doi.org/10.1038/s41586-021-03911-7 (2021).
2. Hoglinger, G. U., Respondek, G. & Kovacs, G. G. New classification of tauopathies. *Rev. Neurol. (Paris)* **174**, 664–668. https://doi.org/10.1016/j.neurol.2018.07.001 (2018).
3. Kovacs, G. G. Tauopathies. *Handb. Clin. Neurol.* **145**, 355–368. https://doi.org/10.1016/B978-0-12-802395-2.00025-0 (2017).
4. Braak, H. & Del Tredici, K. Neuroanatomy and pathology of sporadic Alzheimer's disease. *Adv. Anat. Embryol. Cell Biol.* **215**, 1–162 (2015).
5. Goedert, M. & Spillantini, M. G. Ordered assembly of tau protein and neurodegeneration. *Adv. Exp. Med. Biol.* **1184**, 3–21. https://doi.org/10.1007/978-981-32-9358-8_1 (2019).
6. Duyckaerts, C. *et al.* Seeding and propagation of lesions in neurodegenerative diseases: A new paradigm. *Bull. Acad. Natl. Med.* **199**, 809–819 (2015).
7. DeTure, M. A. & Dickson, D. W. The neuropathological diagnosis of Alzheimer's disease. *Mol. Neurodegener.* **14**, 32. https://doi.org/10.1186/s13024-019-0333-5 (2019).
8. Arnsten, A. F. T., Datta, D. & Preuss, T. M. Studies of aging nonhuman primates illuminate the etiology of early-stage Alzheimer's-like neuropathology: An evolutionary perspective. *Am. J. Primatol.* **83**, e23254. https://doi.org/10.1002/ajp.23254 (2021).
9. Braak, H. & Braak, E. Argyrophilic grains: characteristic pathology of cerebral cortex in cases of adult onset dementia without Alzheimer changes. *Neurosci. Lett.* **76**, 124–127. https://doi.org/10.1016/0304-3940(87)90204-7 (1987).
10. Tolnay, M. & Probst, A. Argyrophilic grain disease. *Handb. Clin. Neurol.* **89**, 553–563. https://doi.org/10.1016/S0072-9752(07)01251-1 (2008).
11. Ferrer, I., Santpere, G. & van Leeuwen, F. W. Argyrophilic grain disease. *Brain* **131**, 1416–1432. https://doi.org/10.1093/brain/awm305 (2008).
12. Ferrer, I. *et al.* Glial and neuronal tau pathology in tauopathies: Characterization of disease-specific phenotypes and tau pathology progression. *J. Neuropathol. Exp. Neurol.* **73**, 81–97. https://doi.org/10.1097/NEN.0000000000000030 (2014).
13. Crary, J. F. *et al.* Primary age-related tauopathy (PART): A common pathology associated with human aging. *Acta Neuropathol.* **128**, 755–766. https://doi.org/10.1007/s00401-014-1349-0 (2014).
14. Kovacs, G. G. Invited review: Neuropathology of tauopathies: Principles and practice. *Neuropathol. Appl. Neurobiol.* **41**, 3–23. https://doi.org/10.1111/nan.12208 (2015).
15. Kovacs, G. G. *et al.* Aging-related tau astrogliopathy (ARTAG): harmonized evaluation strategy. *Acta Neuropathol.* **131**, 87–102. https://doi.org/10.1007/s00401-015-1509-x (2016).
16. Ferrer, I. *et al.* Aging-related tau astrogliopathy (ARTAG): Not only tau phosphorylation in astrocytes. *Brain Pathol.* **28**, 965–985. https://doi.org/10.1111/bpa.12593 (2018).
17. Rosler, T. W. *et al.* Four-repeat tauopathies. *Prog. Neurobiol.* **180**, 101644. https://doi.org/10.1016/j.pneurobio.2019.101644 (2019).
18. Goedert, M., Masuda-Suzukake, M. & Falcon, B. Like prions: the propagation of aggregated tau and alpha-synuclein in neurodegeneration. *Brain* **140**, 266–278. https://doi.org/10.1093/brain/aww230 (2017).
19. Ahmed, Z. *et al.* A novel in vivo model of tau propagation with rapid and progressive neurofibrillary tangle pathology: the pattern of spread is determined by connectivity, not proximity. *Acta Neuropathol.* **127**, 667–683. https://doi.org/10.1007/s00401-014-1254-6 (2014).
20. Clavaguera, F. *et al.* Transmission and spreading of tauopathy in transgenic mouse brain. *Nat. Cell. Biol.* **11**, 909–913. https://doi.org/10.1038/ncb1901 (2009).
21. Clavaguera, F. *et al.* Brain homogenates from human tauopathies induce tau inclusions in mouse brain. *Proc. Natl. Acad. Sci. USA* **110**, 9535–9540. https://doi.org/10.1073/pnas.1301175110 (2013).
22. Boluda, S. *et al.* Differential induction and spread of tau pathology in young PS19 tau transgenic mice following intracerebral injections of pathological tau from Alzheimer's disease or corticobasal degeneration brains. *Acta Neuropathol.* **129**, 221–237. https://doi.org/10.1007/s00401-014-1373-0 (2015).
23. Ferrer, I., Andres-Benito, P., Carmona, M. & Del Rio, J. A. Common and specific marks of different tau strains following intra-hippocampal injection of AD, PiD, and GGT inoculum in htau transgenic mice. *Int. J. Mol. Sci.* https://doi.org/10.3390/ijms232415940 (2022).
24. Audouard, E. *et al.* High-molecular-weight paired helical filaments from alzheimer brain induces seeding of wild-type mouse tau into an argyrophilic 4r tau pathology in vivo. *Am. J. Pathol.* **186**, 2709–2722. https://doi.org/10.1016/j.ajpath.2016.06.008 (2016).
25. Guo, J. L. *et al.* Unique pathological tau conformers from Alzheimer's brains transmit tau pathology in nontransgenic mice. *J. Exp. Med.* **213**, 2635–2654. https://doi.org/10.1084/jem.20160833 (2016).
26. Narasimhan, S. *et al.* Pathological tau strains from human brains recapitulate the diversity of tauopathies in nontransgenic mouse brain. *J. Neurosci.* **37**, 11406–11423. https://doi.org/10.1523/JNEUROSCI.1230-17.2017 (2017).
27. Ferrer, I. *et al.* Familial globular glial tauopathy linked to MAPT mutations: molecular neuropathology and seeding capacity of a prototypical mixed neuronal and glial tauopathy. *Acta Neuropathol.* **139**, 735–771. https://doi.org/10.1007/s00401-019-02122-9 (2020).
28. Ferrer, I., Andres-Benito, P., Sala-Jarque, J., Gil, V. & Del Rio, J. A. Capacity for seeding and spreading of argyrophilic grain disease in a wild-type murine model; comparisons with primary age-related tauopathy. *Front. Mol. Neurosci.* **13**, 101. https://doi.org/10.3389/fnmol.2020.00101 (2020).
29. Weitzman, S. A. *et al.* Insoluble tau from human FTDP-17 cases exhibit unique transmission properties in vivo. *J. Neuropathol. Exp. Neurol.* **79**, 941–949. https://doi.org/10.1093/jnen/nlaa086 (2020).
30. Andres-Benito, P. *et al.* Host tau genotype specifically designs and regulates tau seeding and spreading and host tau transformation following intrahippocampal injection of identical tau AD inoculum. *Int. J. Mol. Sci.* https://doi.org/10.3390/ijms23020718 (2022).
31. Stamelou, M. LRP1: a novel mediator of tau uptake. *Mov. Disord.* **35**, 1136. https://doi.org/10.1002/mds.28107 (2020).
32. Rauch, J. N. *et al.* LRP1 is a master regulator of tau uptake and spread. *Nature* **580**, 381–385. https://doi.org/10.1038/s41586-020-2156-5 (2020).
33. Corbett, G. T. *et al.* PrP is a central player in toxicity mediated by soluble aggregates of neurodegeneration-causing proteins. *Acta Neuropathol.* **139**, 503–526. https://doi.org/10.1007/s00401-019-02114-9 (2020).

34. Legname, G. & Scialo, C. On the role of the cellular prion protein in the uptake and signaling of pathological aggregates in neurodegenerative diseases. *Prion* **14**, 257–270. https://doi.org/10.1080/19336896.2020.1854034 (2020).
35. Celauro, L. *et al.* Different tau fibril types reduce prion level in chronically and de novo infected cells. *J. Biol. Chem.* https://doi.org/10.1016/j.jbc.2023.105054 (2023).
36. Chen, C. *et al.* Pathological Tau transmission initiated by binding lymphocyte-activation gene 3. *BioRxiv.* https://doi.org/10.1101/2023.05.16.541015 (2023).
37. Chen, C. *et al.* Lymphocyte-activation gene 3 facilitates pathological tau neuron-to-neuron transmission. *Adv. Sci. (Weinh).* https://doi.org/10.1002/advs.202303775 (2024).
38. Lima, F. R. *et al.* Cellular prion protein expression in astrocytes modulates neuronal survival and differentiation. *J. Neurochem.* **103**, 2164–2176. https://doi.org/10.1111/j.1471-4159.2007.04904.x (2007).
39. Moser, M., Colello, R. J., Pott, U. & Oesch, B. Developmental expression of the prion protein gene in glial cells. *Neuron* **14**, 509–517. https://doi.org/10.1016/0896-6273(95)90307-0 (1995).
40. Adle-Biassette, H. *et al.* Immunohistochemical expression of prion protein (PrPC) in the human forebrain during development. *J. Neuropathol. Exp. Neurol.* **65**, 698–706. https://doi.org/10.1097/01.jnen.0000228137.10531.72 (2006).
41. Bribian, A. *et al.* Role of the cellular prion protein in oligodendrocyte precursor cell proliferation and differentiation in the developing and adult mouse CNS. *PLoS One* **7**, e33872. https://doi.org/10.1371/journal.pone.0033872 (2012).
42. Lauren, J., Gimbel, D. A., Nygaard, H. B., Gilbert, J. W. & Strittmatter, S. M. Cellular prion protein mediates impairment of synaptic plasticity by amyloid-beta oligomers. *Nature* **457**, 1128–1132. https://doi.org/10.1038/nature07761 (2009).
43. Resenberger, U. K., Winklhofer, K. F. & Tatzelt, J. Cellular prion protein mediates toxic signaling of amyloid beta. *Neurodegener. Dis.* **10**, 298–300. https://doi.org/10.1159/000332596 (2012).
44. Resenberger, U. K. *et al.* The cellular prion protein mediates neurotoxic signalling of beta-sheet-rich conformers independent of prion replication. *EMBO J.* **30**, 2057–2070. https://doi.org/10.1038/emboj.2011.86 (2011).
45. Ganzinger, K. A. *et al.* Single-molecule imaging reveals that small amyloid-beta1-42 oligomers interact with the cellular prion protein (PrP(C)). *Chembiochem* **15**, 2515–2521. https://doi.org/10.1002/cbic.201402377 (2014).
46. Ferreira, D. G. *et al.* alpha-synuclein interacts with PrP(C) to induce cognitive impairment through mGluR5 and NMDAR2B. *Nat. Neurosci.* **20**, 1569–1579. https://doi.org/10.1038/nn.4648 (2017).
47. Salazar, S. V. & Strittmatter, S. M. Cellular prion protein as a receptor for amyloid-beta oligomers in Alzheimer's disease. *Biochem. Biophys. Res. Commun.* **483**, 1143–1147. https://doi.org/10.1016/j.bbrc.2016.09.062 (2017).
48. Urrea, L. *et al.* Involvement of cellular prion protein in alpha-synuclein transport in neurons. *Mol. Neurobiol.* **55**, 1847–1860. https://doi.org/10.1007/s12035-017-0451-4 (2018).
49. Zhang, Y. *et al.* Cellular prion protein as a receptor of toxic amyloid-beta42 oligomers is important for Alzheimer's disease. *Front. Cell Neurosci.* **13**, 339. https://doi.org/10.3389/fncel.2019.00339 (2019).
50. Thom, T. *et al.* Cellular prion protein mediates alpha-synuclein uptake, localization, and toxicity in vitro and in vivo. *Mov. Disord.* **37**, 39–51. https://doi.org/10.1002/mds.28774 (2022).
51. Del Rio, J. A., Ferrer, I. & Gavin, R. Role of cellular prion protein in interneuronal amyloid transmission. *Prog. Neurobiol.* **165–167**, 87–102. https://doi.org/10.1016/j.pneurobio.2018.03.001 (2018).
52. Ondrejcak, T. *et al.* Cellular prion protein mediates the disruption of hippocampal synaptic plasticity by soluble tau in vivo. *J Neurosci* **38**, 10595–10606. https://doi.org/10.1523/JNEUROSCI.1700-18.2018 (2018).
53. Chesebro, B. *et al.* Anchorless prion protein results in infectious amyloid disease without clinical scrapie. *Science* **308**, 1435–1439. https://doi.org/10.1126/science.1110837 (2005).
54. Nuvolone, M. *et al.* Strictly co-isogenic C57BL/6J-Prnp-/- mice: A rigorous resource for prion science. *J. Exp. Med.* **213**, 313–327. https://doi.org/10.1084/jem.20151610 (2016).
55. Manni, G. *et al.* The cellular prion protein beyond prion diseases. *Swiss. Med. Wkly.* **150**, w20222. https://doi.org/10.4414/smw.2020.20222 (2020).
56. Gavin, R., Lidon, L., Ferrer, I. & Del Rio, J. A. The quest for cellular prion protein functions in the aged and neurodegenerating brain. *Cells.* https://doi.org/10.3390/cells9030591 (2020).
57. Watts, J. C., Bourkas, M. E. C. & Arshad, H. The function of the cellular prion protein in health and disease. *Acta Neuropathol.* **135**, 159–178. https://doi.org/10.1007/s00401-017-1790-y (2018).
58. Scialo, C. & Legname, G. The role of the cellular prion protein in the uptake and toxic signaling of pathological neurodegenerative aggregates. *Prog. Mol. Biol. Transl. Sci.* **175**, 297–323. https://doi.org/10.1016/bs.pmbts.2020.08.008 (2020).
59. Scialo, C. *et al.* The cellular prion protein increases the uptake and toxicity of TDP-43 fibrils. *Viruses* https://doi.org/10.3390/v13081625 (2021).
60. Ferrer, I. *et al.* Involvement of oligodendrocytes in tau seeding and spreading in tauopathies. *Front. Aging Neurosci.* **11**, 112. https://doi.org/10.3389/fnagi.2019.00112 (2019).
61. Jiang, Z. *et al.* A nonhuman primate model with Alzheimer's disease-like pathology induced by hippocampal overexpression of human tau. *Alzheimers Res. Ther.* **16**, 22. https://doi.org/10.1186/s13195-024-01392-0 (2024).
62. Villa Gonzalez, M. *et al.* Focal cerebral ischemia induces changes in oligodendrocytic tau isoforms in the damaged area. *Glia* **68**, 2471–2485. https://doi.org/10.1002/glia.23865 (2020).
63. He, B., Chen, W., Zeng, J., Tong, W. & Zheng, P. MicroRNA-326 decreases tau phosphorylation and neuron apoptosis through inhibition of the JNK signaling pathway by targeting VAV1 in Alzheimer's disease. *J. Cell Physiol.* **235**, 480–493. https://doi.org/10.1002/jcp.28988 (2020).
64. Robert, A., Scholl, M. & Vogels, T. Tau seeding mouse models with patient brain-derived aggregates. *Int. J. Mol. Sci.* https://doi.org/10.3390/ijms22116132 (2021).
65. Hosokawa, M. *et al.* Development of a novel tau propagation mouse model endogenously expressing 3 and 4 repeat tau isoforms. *Brain* **145**, 349–361. https://doi.org/10.1093/brain/awab289 (2022).
66. Sanders, D. W. *et al.* Distinct tau prion strains propagate in cells and mice and define different tauopathies. *Neuron* **82**, 1271–1288. https://doi.org/10.1016/j.neuron.2014.04.047 (2014).
67. Tarutani, A. *et al.* Human tauopathy-derived tau strains determine the substrates recruited for templated amplification. *Brain* **144**, 2333–2348. https://doi.org/10.1093/brain/awab091 (2021).
68. Wei, Y., Liu, M. & Wang, D. The propagation mechanisms of extracellular tau in Alzheimer's disease. *J. Neurol.* **269**, 1164–1181. https://doi.org/10.1007/s00415-021-10573-y (2022).
69. Fioriti, L. *et al.* The neurotoxicity of prion protein (PrP) peptide 106–126 is independent of the expression level of PrP and is not mediated by abnormal PrP species. *Mol. Cell Neurosci.* **28**, 165–176. https://doi.org/10.1016/j.mcn.2004.09.006 (2005).
70. Gavin, R. *et al.* PrP(106–126) activates neuronal intracellular kinases and Egr1 synthesis through activation of NADPH-oxidase independently of PrPc. *FEBS Lett.* **579**, 4099–4106. https://doi.org/10.1016/j.febslet.2005.06.037 (2005).
71. Scott-McKean, J. J. *et al.* Soluble prion protein and its N-terminal fragment prevent impairment of synaptic plasticity by Abeta oligomers: Implications for novel therapeutic strategy in Alzheimer's disease. *Neurobiol. Dis.* **91**, 124–131. https://doi.org/10.1016/j.nbd.2016.03.001 (2016).
72. Li, Z., Yin, B., Zhang, S., Lan, Z. & Zhang, L. Targeting protein kinases for the treatment of Alzheimer's disease: Recent progress and future perspectives. *Eur. J. Med. Chem.* **261**, 115817. https://doi.org/10.1016/j.ejmech.2023.115817 (2023).

73. Holubiec, M. I., Gellert, M. & Hanschmann, E. M. Redox signaling and metabolism in Alzheimer's disease. *Front. Aging Neurosci.* **14**, 1003721. https://doi.org/10.3389/fnagi.2022.1003721 (2022).
74. La Vitola, P. *et al.* Cellular prion protein neither binds to alpha-synuclein oligomers nor mediates their detrimental effects. *Brain* **142**, 249–254. https://doi.org/10.1093/brain/awy318 (2019).
75. Balducci, C. *et al.* Synthetic amyloid-beta oligomers impair long-term memory independently of cellular prion protein. *Proc. Natl. Acad. Sci. USA* **107**, 2295–2300. https://doi.org/10.1073/pnas.0911829107 (2010).
76. Calella, A. M. *et al.* Prion protein and Abeta-related synaptic toxicity impairment. *EMBO Mol. Med.* **2**, 306–314. https://doi.org/10.1002/emmm.201000082 (2010).
77. Cisse, M. *et al.* Ablation of cellular prion protein does not ameliorate abnormal neural network activity or cognitive dysfunction in the J20 line of human amyloid precursor protein transgenic mice. *J. Neurosci.* **31**, 10427–10431. https://doi.org/10.1523/JNEUROSCI.1459-11.2011 (2011).
78. Nicoll, A. J. *et al.* Amyloid-beta nanotubes are associated with prion protein-dependent synaptotoxicity. *Nat. Commun.* **4**, 2416. https://doi.org/10.1038/ncomms3416 (2013).
79. Dawson, H. N. *et al.* Inhibition of neuronal maturation in primary hippocampal neurons from tau deficient mice. *J. Cell Sci.* **114**, 1179–1187. https://doi.org/10.1242/jcs.114.6.1179 (2001).
80. Allen, B. *et al.* Abundant tau filaments and nonapoptotic neurodegeneration in transgenic mice expressing human P301S tau protein. *J. Neurosci.* **22**, 9340–9351. https://doi.org/10.1523/JNEUROSCI.22-21-09340.2002 (2002).
81. Yoshiyama, Y. *et al.* Synapse loss and microglial activation precede tangles in a P301S tauopathy mouse model. *Neuron* **53**, 337–351. https://doi.org/10.1016/j.neuron.2007.01.010 (2007).
82. Tuzi, N. L. *et al.* Cre-loxP mediated control of PrP to study transmissible spongiform encephalopathy diseases. *Genesis* **40**, 1–6. https://doi.org/10.1002/gene.20046 (2004).
83. Dubois, N. C., Hofmann, D., Kaloulis, K., Bishop, J. M. & Trumpp, A. Nestin-Cre transgenic mouse line Nes-Cre1 mediates highly efficient Cre/loxP mediated recombination in the nervous system, kidney, and somite-derived tissues. *Genesis* **44**, 355–360. https://doi.org/10.1002/dvg.20226 (2006).
84. Perciedu Sert, N. *et al.* Reporting animal research: Explanation and elaboration for the ARRIVE guidelines 2.0. *PLoS Biol* **18**, e3000411. https://doi.org/10.1371/journal.pbio.3000411 (2020).
85. Aminoff, M. J. & Daroff, R. B. *Encyclopedia of the neurological sciences* (Academic Press/Elsevier, 2014).
86. Mai, J. R. K., Assheuer, J. & Paxinos, G. *Atlas of the human brain* (Academic Press, 1997).
87. Jicha, G. A., Bowser, R., Kazam, I. G. & Davies, P. Alz-50 and MC-1, a new monoclonal antibody raised to paired helical filaments, recognize conformational epitopes on recombinant tau. *J. Neurosci. Res.* **48**, 128–132. https://doi.org/10.1002/(sici)1097-4547 (1997).

Acknowledgements
The authors thank Tom Yohannan for his editorial advice. We also thank Miriam Segura-Feliu and Juan José López for their technical help. The authors thank all the members of the Del Río, Ferrer, Ávila, and Aguzzi laboratories for their helpful comments.

Author contributions
J.S.-J., V.G., P.A.-B., I.M.-S., P.P.-P. and J.A.D.R. performed experiments and data analysis. J.A., M.N., J.L.L., A.A., R.G. and I.F. and J.A.D.R. designed the experiments. J.A.D.R. and I.F. write and edited the manuscript. All authors contributed to the article and approved the submitted version.

Funding
J.A. del Río and R. Gavín were supported by PRPCDEVTAU PID2021-123714OB-I00, ALTERNed PLEC2022-009401, PDC2022-133268-I00 and ADNano from Plan Complementario de Biotecnología Aplicada a la Salud (C17.I1) funded by *MCIN/AEI/10.13039/501100011033 and by "ERDF A way of making Europe"*, the CERCA Programme, and by the Commission for Universities and Research of the Department of Innovation, Universities, and Enterprise of the Generalitat de Catalunya (SGR2021-00453). The project leading to these results received funding from "la Caixa" Foundation (ID 100010434) under the agreement LCF/PR/HR19/52160007 to JADR and IF. V. Gil was supported by the María de Maeztu Unit of Excellence (Institute of Neurosciences, University of Barcelona) MDM-2017-0729. J. Sala-Jarque was supported by the Tatiana Pérez de Guzmán el Bueno Foundation. I. Martínez-Soria was supported by MICINN (FPI Programme, PRE2022-103197) and P. Picón-Pagès was supported by Ciberned.

Competing interests
The authors declare no competing interests.

Additional information
Supplementary Information The online version contains supplementary material available at https://doi.org/10.1038/s41598-024-72232-2.

Correspondence and requests for materials should be addressed to J.A.d.R.

Reprints and permissions information is available at www.nature.com/reprints.

Publisher's note Springer Nature remains neutral with regard to jurisdictional claims in published maps and institutional affiliations.